Ionizing wave via high-power HF acceleration

Evgeny Mishin and Todd Pedersen
Space Vehicles Directorate, Air Force Research Laboratory, Hanscom AFB, MA, USA

Abstract. Recent ionospheric modification experiments with the 3.6 MW transmitter at the High Frequency Active Auroral Research Program (HAARP) facility in Alaska led to discovery of artificial ionization descending from the nominal interaction altitude in the background F-region ionosphere by $\sim$60 km. This paper presents a physical model of an ionizing wavefront created by suprathermal electrons accelerated by the HF-excited plasma turbulence.

Introduction

High-power HF radio waves can excite electrostatic waves in the ionosphere near altitudes where the injected wave frequency f_0 matches either the local plasma frequency $f_p \approx 9\sqrt{n_e}$ kHz (the density n_e in cm^{-3}) or the upper hybrid resonance $f_{uhr} = \sqrt{f_p^2 + f_c^2}$ (f_c is the electron cyclotron frequency) [e.g., *Gurevich*, 1978]. The generated waves increase the bulk electron temperature to T_e =0.3-0.4 eV, while some electrons are accelerated to suprathermal energies $\varepsilon = \frac{1}{2}mv^2$ up to a few dozen eV [e.g., *Carlson et al.*, 1982; *Rietveld et al.*, 2003]. Upon impact with neutrals (N_2, O_2, O), suprathermal electrons excite optical emissions termed Artificial Aurora (AA) [e.g., *Bernhardt et al.*, 1989; *Gustavsson and Eliasson*, 2008].

Heating-induced plasma density modifications are usually described in terms of chemical and transport processes [e.g., *Bernhardt et al.*, 1989; *Djuth et al.*, 1994; *Dhillon and Robinson*, 2005; *Ashrafi et al.*, 2006]. However, the *Pedersen et al.* [2009; 2010] discovery of rapidly descending plasma layers seems to point to additional mechanisms. *Pedersen et al.* [2010, hereafter P10] suggested that the artificial plasma is able to sustain interaction with the transmitted HF beam and that the interaction region propagates (downward) as an ionizing wavefront. In this paper, the formation of such downward-propagating ionizing front is ascribed to suprathermal electrons accelerated by the HF-excited plasma turbulence.

Ionizing wave

The descending feature is evident in Figure 1, which is representative of P10 Fig. 3 with the regions of ion-line (IL) radar echoes from the MUIR incoherent scatter radar (courtesy of Chris Fallen) overlaid [c.f. *Oyama et al.*, 2006]. Shown are sequential altitude profiles of the green-line emissions (λ =557.7 nm, excitation potential $\varepsilon_g \approx$4.2 eV) observed at the HAARP facility on 17 March 2009. Here, the O-mode radio beam was injected into the magnetic zenith (MZ), i.e. along the magnetic field $\mathbf{B}_0$, at the effective radiative power P_0[MW] $\approx$440 and frequency f_0 =2.85 MHz ($2f_c$ at $h_{2f_c} \approx$230 km). The contours of $f_p = f_0$ or $n_e = n_c \approx 10^5$ cm^{-3} (cyan) and $f_{uhr} = f_0$ (violet) are inferred from ionograms acquired at 1 min intervals [P10 Fig. 3]. The regions of enhanced IL are shown in green color. Note, the blue-line emissions at 427.8 nm (not shown) coincided with the green-line emissions, as seen looking from the HAARP site [P10].

During the first 2 min in the heating, the artificial plasma is confined to the bottomside of the F layer at altitudes h >180 km. The corresponding descent of the IL scatter is similar to that described by *Dhillon and Robinson* [2005] and *Ashrafi et al.* [2006]. A sudden brightening of AA and increased speed of descent of the artificial plasma 'layer' (patch) in the HF-beam center occurs near 180 km, while its peak plasma frequency $foFa$ reaches f_0. In fact, the optical data shows [P10] that this patch is fairly uniform near $\sim$180 km but then becomes a $\sim$20-km collection of ($\|\mathbf{B}_0$) filaments a few km in diameter. While the degree of inhomogeneity of the descending patch increases, its speed, $V_{obs} \simeq$0.3
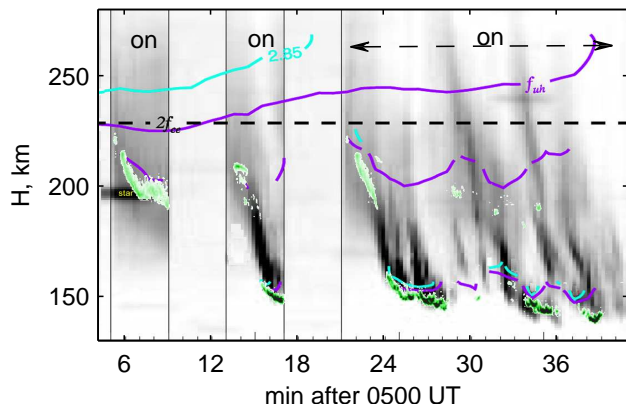
Figure 1. Time-vs-altitude plot of 557.7 nm optical emissions (black color) along $\mathbf{B}_0$. Blue (violet) lines indicate the matching altitudes $f_0 = f_p$ (f_{uh}). The dashed line indicates h_{2f_c}. The transmitter on periods are indicated. Shown in green is the MUIR IL intensity (courtesy of Chris Fallen). Horizontal blips are stars passing through the view.

km/s, appears to be constant until ≈ 160 km. Then, the artificial plasma slows down, staying near the terminal altitude $h_{\min} \approx 150$ km before the emissions retreat in altitude near the end of 4-min injection pulse. During a continuous 'on' period, the artificial plasma near $h_{\min}$ was quenched several times, initiating the process over again from higher altitudes.

Hereafter, we focus on the descending feature at $h \leq 180$ km where $foFa \geq f_0$ or $n_e \geq n_c$. Enhanced 427.8-nm emissions indicate the presence of electrons with energies $\varepsilon > \varepsilon_b \approx 18.7$ eV, exceeding the ionization energies of N_2, O_2, and O. The ionization rate q_a is given by

$$dn_e/dt = q_a = n_a \cdot \langle \nu_{ion}(\varepsilon) \rangle \qquad (1)$$

where ν_{ion} is the ionization frequency, and $\langle ... \rangle$ means averaging over the accelerated distribution of the density n_a. Hereafter, we employ *Majeed and Strickland's* [1997] electron impact cross-sections and the *Hedin* [1991] MSIS90 model for the densities $[N_2]$, $[O]$, and $[O_2]$ on 17 March 2009.

At each time step t_i, artificial ionization occurs near the critical altitude $h_c(t_i)$, defined from the condition $n_e(h_c) = n_c$. The density profile just below h_c is represented as follows

$$n_e(x, t_i) = n_c \cdot \Psi(x) \qquad (2)$$

Here $x = \xi/L_\parallel$, $\xi = (h_c - h)/\cos\alpha_0$ is the distance along $\mathbf{B}_0$, α_0 is the conjugate of the magnetic dip angle ($\approx 15°$ at HAARP), and $L_\parallel$ is the ($\parallel \mathbf{B}_0$) extent of the ionization region. $\Psi(x)$ is a monotonic function satisfying the conditions $\Psi(0) \geq 1$ and $\Psi(x) \ll 1$ at $x > 1$, since the ambient plasma density $n_0 \ll n_c$ at $h \leq 180$ km. As the ratio $\delta_e(\varepsilon)$ of inelastic (ν_{il}) to elastic (ν_{el}) collision frequencies is small, the accelerated electrons undergo fast isotropization due to elastic scattering and thus $L_\parallel \simeq \left\langle l_{ion}\sqrt{\delta_e/2} \right\rangle$, where $l_{ion} = v/\nu_{ion}$ [c.f. *Gurevich et al.*, 1985].

Evidently, as soon as at some point $x_i \leq 1$ the density $n_e(x_i, t_i + \Delta t) \simeq q_a(\xi_i) \cdot \Delta t$ reaches n_c, the critical height shifts to this point, i.e. $h_c(t_{i+1}) \simeq h_c(t_i) - L_\parallel \cdot x$. These conditions define the ionization time, $T_{ion}^{-1} \simeq q_a/n_c$, and the speed of descent

$$V_d = |dh_c/dt| \simeq L_\parallel T_{ion}^{-1} \simeq \left\langle v\sqrt{\delta_e/2} \right\rangle n_a/n_c \qquad (3)$$

Note, eq. (3) contains no dependence on the total neutral density N_n and hence predicts $V_d \simeq \text{const}(h)$, if the same distribution of accelerated electrons is created at each step. As $\left\langle \delta_e^{1/2} v \right\rangle \simeq 1.5 \cdot 10^6$ m/s, we get from eq. (3) that the value of V_d (3) matches V_{obs} at $n_a = n_a^{(d)} \simeq 6 \cdot 10^{-4} n_c$ or $n_a^{(d)} \simeq 60$ cm^{-3}.

Discussion and conclusions

We now turn to justify this acceleration-ionization-descent scenario. Enhanced IL echoes, like in Figure 1, usually result from the parametric decay instability (PDI$_l$) and oscillating two stream instability (OTSI) of the pump wave near the plasma resonance [e.g., *Mjølhus et al.*, 2003]. The latter develops if the relative pump wave energy density $\widetilde{W}_0 = \left| E_0^2 \right| / 8\pi n_c T_e$ exceeds $\widetilde{W}_{th} \simeq \frac{2}{kL_n} + \frac{4\nu_T}{\omega_0}$, where k is the plasma wave number, ν_T is the collision frequency of thermal electrons, and $L_n^{-1} = |\nabla \ln n_e|$. The free space field of the pump wave is $E_{fs} \approx 5.5\sqrt{P_0}/r \approx 0.65$ V/m at $r = 180$ km (at the HF-beam center) or $\widetilde{W}_{fs} \simeq 5 \cdot 10^{-4}$ at $T_e = 0.2$ eV. For incidence angles $\theta < \arcsin\left(\sqrt{f_c/(f_c + f_0)}\sin\alpha_0\right)$, the amplitude in the first Airy maximum is $E_A \approx (2\pi/\sin\alpha_0)^{2/3}(f_0 L_n/c)^{1/6} E_{fs}$ [e.g., *Mjølhus et al.*, 2003] or $\widetilde{W}_A \approx 0.1(L_n/L_0)^{1/3}$, where $L_0 = 30$ km. For injections at MZ, following *Mjølhus et al.* [2003] one gets $\widetilde{W}_A^{(mz)} \approx \widetilde{W}_A/4$.

As $\widetilde{W}_A^{(mz)} \gg \mu$ (the electron-to-ion mass ratio), we get $k \simeq r_D^{-1}\left(\mu\widetilde{W}_A^{(mz)}\right)^{1/4}$ [e.g., *Alterkop et al.*, 1973] or $kr_D \simeq 1/40$ (r_D is the Debye radius) yielding $\widetilde{W}_{th} \simeq 10^{-4}(L_0/L_n)$. The 'instant' gradient-scale

of the artificial layer is $L_n \simeq 3 \rightarrow 1$ km at $180 \rightarrow 150$ km (see below) gives $\widetilde{W}_{th} \approx (1 \rightarrow 3) \cdot 10^{-3}$. Thus, OTSI can easily develop in the first Airy maximum. In turn, PDI_l can develop in as many as $\simeq 30$ Airy maxima over a distance $l_a \simeq 1$ km [c.f. *Djuth*, 1984; *Newman et al.*, 1998]. At $T_e/T_i < 4$, PDI_l is saturated via induced scattering of Langmuir (l) waves, piling them up into 'wave condensate' ($k \rightarrow 0$) [e.g., *Zakharov et al.*, 1976]. The condensate is subject to OTSI, thereby leading to strong (cavitating) turbulence and electron acceleration [e.g., *Galeev et al.*, 1977].

At $W_l/n_0 T_e < (f_c/f_p)^2$, the acceleration results in a power-law ($\|\mathbf{B}_0$) distribution at $\varepsilon_{\max} \geq \varepsilon_\| = \frac{1}{2} m u^2 \geq \varepsilon_{\min}$ [*Galeev et al.*, 1983; *Wang et al.*, 1997]

$$F_a^\|(\varepsilon_\|) \simeq n_a (2p_a - 1)/v_{\min} \cdot (\varepsilon_{\min}/\varepsilon_\|)^{p_a} \qquad (4)$$

where $p_a \simeq 0.75$-1. The density n_a and $\varepsilon_{\min}$ are determined by the wave energy W_l trapped by cavitons and the joining condition with the ambient electron distribution $F_a^\|(\varepsilon_{\min}) = F_0(\varepsilon_{\min})$. If F_0 is a Maxwellian distribution, this gives $\varepsilon_{\min}^m \approx 10 T_e$ and $n_a^m \approx 10^{-4} n_e$. When background suprathermal (s) electrons of the density n_s are present, then $F_0(\varepsilon \gg T_e) \rightarrow F_s(\varepsilon)$ and $\varepsilon_{\min} \simeq 30 \left(n_s T_e / W_l \right)^{2/5}$ eV [e.g., *Mishin et al.*, 2004], yielding $\varepsilon_{\min} \leq 10$ eV at $n_e = n_c$, $\widetilde{W}_l \simeq 10^{-3}$, and $n_s \leq 10$ cm^{-3}. In the ionizing wave, a natural source of the s-electrons is ionization by those accelerated electrons that can propagate from $\xi \sim 0$ to $\xi \sim L_\|$ (see Figure 2).

We can now evaluate the excitation and ionization rates. The column 427.8-nm intensity in Rayleighs (R) is given by

$$I \approx 10^{-6} A_b \int d\xi \int \sigma_b(\varepsilon) \Phi_a(\varepsilon, \xi) d\varepsilon \cdot [N_2(\xi)] \qquad (5)$$

Here σ_b is the excitation cross section of the $N_2^+(^1N)$ state, $A_b \approx 0.19$, $\Phi_a = \frac{2\varepsilon}{m^2} F_a$ is the differential number flux, and $F_a(\varepsilon) \simeq n_a \frac{p_a - 0.5}{2\pi} v_{\min}^{-3} (\varepsilon_{\min}/\varepsilon)^{p_a + 1}$ is an isotropic distribution to which the accelerated distribution $F_a^\|$ (4) is transformed at distances $|\xi| > v/\nu_{el}$ due to elastic scattering [c.f. *Gurevich et al.*, 1985].

Integrating eq. (5) over the energy range $\varepsilon_b \leq \varepsilon \leq 10^2$ eV at $p_a = 0.85$ yields the brightness of a Δh-km column $\Delta I(h_c) \approx 2.5 \cdot 10^{-12} n_a [N_2(h_c)] \cdot \Delta h$ R near altitude h_c, given that $\Delta h \ll H_n \simeq 8$ km (the atmosphere scale-height). The total intensity I is defined by the vertical extent of the (excitation) layer Δ_b, where $\varepsilon(\xi) \geq \varepsilon_b$. It can be evaluated using the *Majeed and Strickland* [1997] loss function $L(\varepsilon) = \sum_j L_j(\varepsilon)$ with j designating N_2, O_2, and O. Outside the acceleration layer, i.e. $|\xi| > l_a$,
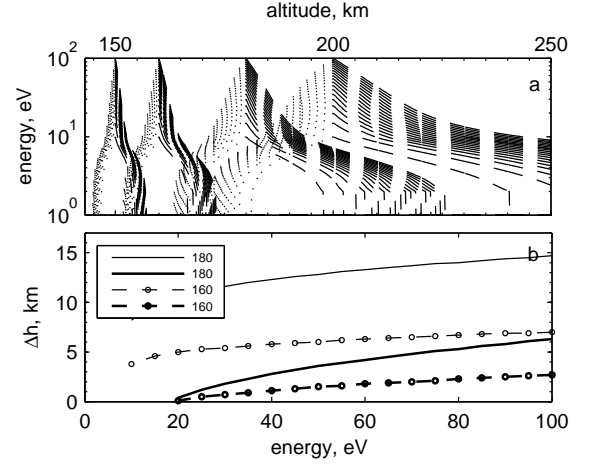
Figure 2. (a) Altitude profiles $\varepsilon(\varepsilon_0, \xi)$ at $\varepsilon_0 = 10$, 15, ...100 eV and $h_0 = 150$, ...200 km. (b) Half-widths Δ_g (thin lines) and Δ_b (thick) of the green- and blue-line excitation layers near $h_c = 160$ (circles) and 180 (solid lines) km.

the energy of an electron of the initial energy ε_0 at a distance ξ from the origination point h_0 is

$$\varepsilon(\varepsilon_0, \xi) \simeq \varepsilon_0 - \int_{h_0}^{h_0 + \xi} L(\varepsilon(z)) \sqrt{2/\delta_e(\varepsilon(z))} dz \qquad (6)$$

Figure 2a presents the results of calculations of eq. (6) for $\varepsilon_0 = 10$, 15, ... 10^2 eV and $h_0 = 150$, 160, 180, and 200 km. The altitude profiles at $\varepsilon \geq 5$ eV and hence the layers of excitation/ionization are nearly symmetric about h_0 at $h \leq 180$ km. Panel b shows the half-widths Δ_g and Δ_b of the green- and blue-line excitation layers about $h_c = 180$ and 160 km as function of ε_0. The half-width of the ionization layer Δ_{ion} (not shown) is $\approx \Delta_b$ at $\varepsilon_0 > 20$ eV. Since $\Delta_b < H_n$, we can estimate the 427.8-nm intensity at $h_c = 180 \rightarrow 160$ km as $I|_{h_c} \simeq 5 \cdot 10^{-12} n_a \cdot [N_2(h_c)] \langle \Delta_b(h_c) \rangle \simeq (0.16 \rightarrow 0.2) \cdot n_a$ R. Comparing $I|_{h_c}$ with the spatially-averaged intensities $\widehat{I}_b \approx 10 \rightarrow 5$ R [P10 Fig. 1] yields $\widehat{n}_a \simeq 60 \rightarrow 25$ cm^{-3}. Note that $\widehat{n}_a \approx n_a^{(d)}$ at 180 km, in agreement with a uniform structure, while spatial averaging underestimates n_a inside the $\sim$km-scale filaments at 160 km.

Calculating the ionization frequency in eq. (1) with $F_a(\varepsilon)$ gives $\langle \nu_{ion} \rangle \approx \kappa_{ion}^* \cdot \left([N_2] + \frac{1}{2}[O] + 0.95[O_2] \right)$ s^{-1}, where $\kappa_{ion}^* = \langle v\sigma_{ion} \rangle / n_a \approx 1.8 \cdot 10^{-8}$ cm^{3}s^{-1} is the coefficient of ionization of N_2. The total ionization rate $q_a^{(d)} \sim 10^4$ cm^{-3}s^{-1} greatly exceeds recombination losses $\approx 10^{-7} n_c^2 \approx 10^3$ cm^{-3}s^{-1} (the main ion component at these altitudes is NO^+). This justifies the use
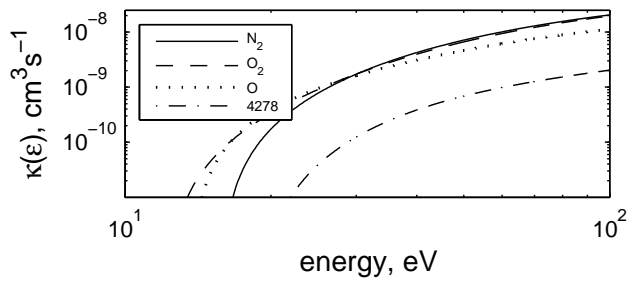
Figure 3. The ionization coefficients of N_2, O_2, and O and the excitation coefficient of the $N_2^+(^1N)$ state vs. $\varepsilon_{\max}$.

of eq. (1) for evaluating the artificial plasma density. Taking an average energy loss per ionization $\sim$20 eV results in the column dissipation rate $<$0.1 mW/m^2 or $<$10% of the 440-MW Poynting flux, consistent with P10's estimates.

As shows Figure 3, the coefficients of ionization and blue-line excitation by accelerated electrons decrease by a factor of $\sim$2 (10) between $\varepsilon_{\max} =10^2$ and 50 (30) eV. The Liouville theorem predicts $F(\varepsilon_0 - \Delta\varepsilon(\varepsilon_0, \xi), h_0 + \xi) = F_0(\varepsilon_0, h_0)$, where $\Delta\varepsilon(\varepsilon_0, \xi)$ is given by the integral in eq. (6). Thus, the gradient scale-length L_n of the artificial plasma is about the distance ξ_{50}, defined by the condition $\Delta\varepsilon(10^2, \xi_{50}) \approx$50 eV. Numerically, we get $\xi_{50} \approx \Delta_b(50)$ or $L_n \approx$3$\rightarrow$1.5 km near $h_c =$180$\rightarrow$160 km and $q_a L_n/n_c \simeq V_{obs}$, as predicted by eq. (3). Note that the artificial plasma density profiles derived from iono-grams indeed have $\sim$1-km gradient scale-lengths near 150 km [c.f. P10 Fig. 2].

Figure 1 shows that the descent slows down below 160 km and ultimately stops at $h_{\min} \approx$150 km. The presence of IL and bright green-line emissions indicate that plasma turbulence is still excited and efficiently ac-celerates electrons above 4 eV. However, the blue-line emissions almost vanish [P10], thereby indicating only few accelerated electrons at $\varepsilon \geq \varepsilon_b$. That this is in no way contradictory follows from the fact that inelastic losses increase tenfold between 10 and 20 eV. Acceler-ation stops at $\varepsilon = \varepsilon_{\max} \ll$100 eV when $\nu_{il}(\varepsilon_{\max})$ ex-ceeds the acceleration rate $mD_\parallel(u_{\max})/8\pi\varepsilon_{\max}$, where $D_\parallel(u) \approx \frac{\omega_p^2}{4n_e m u}\left|E_{k_\parallel}\right|^2$ and $k_\parallel = \omega_p/u$ [*Volokitin and Mishin*, 1979]. The critical neutral density is roughly estimated as $\sim$5$\cdot$10^{11} cm^{-3}, i.e N_n at $\sim$150 km. The fact that the artificial plasma stays near $h_{\min}$ indi-cates that ionization is balanced by recombination or $q_a^{\min} \sim 10^{-7}n_c^2 \approx 0.1q_a^{(d)}$, which at $n_a \sim n_a^{(d)}$ corre-sponds to $\varepsilon_{\max} \approx$30 eV (Figure 3).

A mechanism for generating km-sized filaments be-low 180 km could be the thermal self-focusing insta-bility (SFI) near h_c, resulting in a broad spectrum of plasma irregularity scale sizes [e.g., *Guzdar et al.*, 1998]. Significantly, $\sim$km-scale plasma irregularities grow ini-tially but within 10s of seconds thermal self-focusing leads to smaller (10s to 100s meters) scale sizes. Dur-ing descent, the critical altitude moves downward by several km within 10 s, thereby precluding further de-velopment of SFI, while the $\sim$km-scale irregularities have sufficient time to develop. When the descent rate drops, small-scale irregularities can fully develop and scatter the HF beam, thereby impeding the develop-ment of OTSI/PDI$_L$ and hence ionization. As soon as the artificial plasma decays, SFI falls away and hence irregularities gradually disappear. Then, the artificial plasma can be created again. This explains why the artificial layer ceases and then reappears (Figure 1).

In conclusion, we have shown that the artificial plasma sustaining interaction with the transmitted HF beam can be created via enhanced ionization by suprather-mal electrons accelerated by Langmuir turbulence near the critical altitude. As soon as the interaction region is ionized, it shifts toward the upward-propagating HF beam, thereby creating an ionizing wavefront, which resembles *Pedersen et al.*'s [2010] descending artificial ionospheric layers.

References

Alterkop, B., A. Volokitin, V. Shapiro, and V. Shevchenko (1973), Contribution to the nonlinear theory of the "modified" decay instability, *JETP Let-ters*, *18*, 24.

Ashrafi, M., M. Kosch and F. Honary (2006), Heater-induced altitude descent of the EISCAT UHF ion-line enhancements: Observations and modeling, *Adv. Space Res.*, *38*, 2645.

Bernhardt, P., C. Tepley, and L. Duncan (1989), Air-glow enhancements associated with plasma cavities formed during ionospheric heating experiments, *J. Geophys. Res.*, *94*, 9071.

Carlson, H., V. Wickwar, and G. Mantas (1982), Ob-servations of fluxes of suprathermal electrons accel-

erated by HF excited Langmuir instabilities, *J. Atm. Terr. Phys.*, *12*, 1089.

Djuth, F., (1984), HF-enhanced plasma lines in the lower ionosphere, *Radio Sci.*, *19*, 383.

Djuth., F., P. Stubbe, M. Sulzer, H. Kohl, M. Rietveld, and J. Elder (1994), Altitude characteristics of plasma turbulence excited with Tromsø superheater, *J. Geophys. Res.*, *99*, 333.

Dhillon, R. S., and T. R. Robinson (2005), Observations of time dependence and aspect sensitivity of regions of enhanced UHF backscatter associated with RF heating, *Ann. Geophys.*, *23*, 75.

Galeev, A., R. Sagdeev, V. Shapiro, and V. Shevchenko (1977), Langmuir turbulence and dissipation of high-frequency energy, *Sov. Phys. JETP*, *46*, 711.

Galeev, A., R. Sagdeev, V. Shapiro, and V. Shevehenko (1983), Beam plasma discharge and suprathermal electron tails, in *Active Experiments in Space (Alpbach, Austria)*, SP-195, pp. 151, ESA, Paris.

Gurevich, A., Y. Dimant, G. Milikh, and V. Vaskov (1985), Multiple acceleration of electrons in the regions high-power radio-wave reflection in the ionosphere, *J. Atmos. Terr. Phys.*, *47*, 1057.

Gustavsson, B., and B. Eliasson (2008), HF radio wave acceleration of ionospheric electrons: Analysis of HF-induced optical enhancements, *J. Geophys. Res.*, *113*, A08319, doi:10.1029/2007JA012913.

Guzdar, P. N., P. K. Chaturvedi, K. Papadopoulos, and S. L. Ossakow (1998), The thermal self-focussing instability near the critical surface in the high-latitude ionosphere, *J. Geophys. Res., 103*, 2231.

Hedin, A. (1991), Extension of the MSIS thermospheric model into the middle and lower atmosphere, *J. Geophys. Res.*, *96*, 1159.

Majeed, T., and D. J. Strickland (1997), New survey of electron impact cross sections for photoelectron and auroral electron energy loss calculations, *J. Phys. Chem. Ref. Data*, *26*, 335.

Mishin, E., W. Burke, and T. Pedersen (2004), On the onset of HF-induced airglow at magnetic zenith, *J. Geophys. Res.*, *109*, A02305, doi: 10.1029/2003JA010205.

Mjølhus, E. Helmersen, and D. DuBois (2003), Geometric aspects of HF driven Langmuir turbulence in the ionosphere, *Nonl. Proc. Geophys., 10*, 151.

Newman, D., M. Goldman, F. Djuth, and P. Bernhardt (1998), Langmuir turbulence associated with ionospheric modification: Challenges associated with recent observations during a sporadic-E event, in: *Phys. of Space Plasmas.*, ed. by T. Chang and J. Jaasperse, v. 15, p. 259, MIT, Cambridge, MA.

Oyama, S., B. J. Watkins, F. T. Djuth, M. J. Kosch, P. A. Bernhardt, and C. J. Heinselman (2006), Persistent enhancement of the HF pump-induced plasma line measured with a UHF diagnostic radar at HAARP, *J. Geophys. Res., 111*, A06309, doi:10.1029/2005JA011363.

Pedersen, T., B. Gustavsson, E. Mishin, E. MacKenzie, H. C. Carlson, M. Starks, and T. Mills (2009), Optical ring formation and ionization production in high-power HF heating experiments at HAARP, *Geophys. Res. Lett., 36*, L18107, doi:10.1029/2009GL040047.

Pedersen, T., B. Gustavsson, E. Mishin, E. Kendall, T. Mills, H. C. Carlson, and A. L. Snyder (2010), Creation of artificial ionospheric layers using high-power HF waves, *Geophys. Res. Lett., 37*, L02106, doi:10.1029/ 2009GL041895.

Rietveld, M., M. Kosch, N. Blagoveshchenskaya, V. Kornienko, T. Leyser, and T. Yeoman (2003), Ionospheric electron heating, optical emissions and striations induced by powerful HF radio waves at high latitudes: Aspect angle dependence, *J. Geophys. Res.*, *108*, 1141, doi: 10.1029/2002JA009543.

Wang, J., D. Newman, and M. Goldman (1997), Vlasov simulations of electron heating by Langmuir turbulence near the critical altitude in the radiation-modified ionosphere, *J. A. S. -T. P.*, *59*, 2461.

Volokitin, A., and E. Mishin (1979), Relaxation of an electron beam in a plasma with infrequent collisions, *Sov. J. Plasma Phys. 5*, 654.

Zakharov, V., S. Musher, and A. Rubenchik (1976), Weak Langmuir turbulence of an isothermal plasma, *Sov. Phys. JETP, 42*, 80.

Space Vehicles Directorate, Air Force Research Laboratory, Hanscom AFB, MA 01731 (e-mail: Evgeny.Mishin@hanscom.af.mil; Todd.Pedersen@hanscom.af.mi)